Available online at www.sciencedirect.com
SCIENCE DIRECT®
International Journal of Heat and Mass Transfer 49 (2006) 2642–2651
International Journal of HEAT and MASS TRANSFER
www.elsevier.com/locate/ijhmt

Effect of a magnetic field on the convection of paramagnetic fluid in unstable and stable thermosyphon-like configurations

Elżbieta Fornalik [a,b,c,*], Piotr Filar [b], Toshio Tagawa [a,b], Hiroyuki Ozoe [a,b], Janusz S. Szmyd [c]

[a] Institute for Materials Chemistry and Engineering, Kyushu University, Kasuga Koen 6-1, 816-8580 Fukuoka, Japan
[b] Interdisciplinary Graduate School of Engineering Sciences, Kyushu University, Kasuga Koen 6-1, 816-8580 Fukuoka, Japan
[c] Department of Theoretical Metallurgy and Metallurgical Engineering, AGH University of Science and Technology, 30 Mickiewicz Ave, 30-059 Krakow, Poland

Received 9 July 2004; received in revised form 10 January 2005
Available online 13 March 2006

Abstract

Convection of a paramagnetic fluid inside a vertical cylinder placed in the bore of a superconducting magnet was studied. The bore and the cylinder were placed coaxially. The side wall of a top cylinder was electrically heated, while the side wall of a lower cylinder was cooled by running water through a constant temperature bath. Two configurations were investigated: unstable (the lower side wall heated and the upper one cooled) and stable (the lower wall cooled and the upper wall heated). A mixture of water and glycerol was used as a working fluid, and its magnetic susceptibility was increased by adding $Gd(NO_3)_3 \cdot 6H_2O$. Between the upper and lower side walls a Plexiglas thin cylinder plate was placed. This middle cross-section was illuminated with LED light to visualize the fluid temperature with dispersed liquid crystal slurry. For the unstable configuration, multiple spokes were observed with further increase in the number of spokes with a magnetic field. The magnetic field enhanced the convective flow and also induced flow from a quasi conduction state. The corresponding heat transfer rates were measured with and without a magnetic field. The differences between the stable and unstable configurations of the experimental setup were discussed.

Keywords: Convection; Magnetic field; Paramagnetic fluid; Visualization; Heat transfer rate

1. Introduction

The application of a magnetic field in various research areas has significantly increased in recent years. The development of superconducting magnets has allowed the generation of magnetic fields up to 20 T (or higher with hybrid magnets).

The magnetic field affects the convection of both electro-conducting fluids (liquid metals) and non-electro-conducting fluids (the diamagnetic and paramagnetic fluids). The present report is limited to the latter case.

A strong magnetic field can influence the behavior or movement of non-electro-conducting fluids, on which a weak magnetic field has limited effect. The effect of the magnetic buoyancy force on the convection of paramagnetic fluids was first reported by Braithwaite et al. [2], who described the suppression or enhancement of gravitational convection of paramagnetic fluid by a magnetic field. Many research works have followed. For example, Ikezoe et al. [3] succeeded in droplet levitation not only diamagnetic but also for paramagnetic fluids, while the groups of Wakayama investigated the behavior of air as a paramagnetic fluid in a strong magnetic field. New magneto-aerodynamic phenomena such as airflow generation [13]

* Corresponding author. Address: Department of Theoretical Metallurgy and Metallurgical Engineering, AGH University of Science and Technology, 30 Mickiewicz Ave, 30-059 Krakow, Poland. Tel.: +48 12 617 2663; fax: +48 12 617 2685.
E-mail address: elaf@agh.edu.pl (E. Fornalik).

0017-9310/$ - see front matter © 2006 Elsevier Ltd. All rights reserved.
doi:10.1016/j.ijheatmasstransfer.2005.11.034

Nomenclature

a	internal length of the cubic enclosure (m)
$b = \sqrt{b_r^2 + b_z^2}$	magnetic induction (T)
b_0	reference magnetic induction $= \mu_m i/l$ (T)
b_r	radial component of magnetic induction (T)
b_z	axial component of magnetic induction (T)
$\vec{\nabla} b^2$	gradient of a square of magnetic induction (T^2/m)
$\vec{B} = (\vec{b}/b_0)$	dimensionless magnetic induction (–)
$\vec{\nabla}\lvert B\rvert^2$	dimensionless variable for $\vec{\nabla} b^2$ (–)
B_r	dimensionless horizontal component of magnetic induction $= b_r/b_0$ (–)
B_z	dimensionless axial component of magnetic induction $= b_z/b_0$ (–)
d	cylinder diameter (m)
g	gravitational acceleration (m/s^2)
i	electric current in a magnet coil (A)
I	electric current in a heating coil (A)
l	reference length (m)
Nu	$(Q_{net\_conv}/Q_{net\_cond})$ Nusselt number (–)
Pr	(ν/α) Prandtl number (–)
Q_{cond}	conduction heat flux (W)
Q_{conv}	convection heat flux (W)
Q_{heater}	total heat power (W)
Q_{loss}	heat loss for a cylindrical enclosure (W)
Q_{loss_cubic}	heat loss for a cubical enclosure (W)
Q_{net_cond}	net conduction heat flux (W)
Q_{net_conv}	net convection heat flux (W)
r	radial coordinate (m)
r_0	inner radius of a cylinder (m)
R	(r/r_0) dimensionless radial coordinate (–)
Ra	$(g\beta(\theta_{hot} - \theta_{cold})r_0^3/\alpha\nu)$ Rayleigh number (–)
Ra_0	initial Rayleigh number (without the magnetic field) (–)
Ra_m	$\left(Ra\left[\pm 1 + \gamma\left(1 + (\beta\theta_0)^{-1}\right)B_z(\partial B_z/\partial Z)_{r=0}^{z=0}\right]\right)$ magnetic Rayleigh number (–)
t	time (s)
U	electric voltage for a heating coil (V)
z	axial coordinate (m)
Z	(z/r_0) dimensionless axial coordinate (–)

Greek symbols

α	thermal diffusivity (m^2/s)
β	thermal expansion coefficient (1/K)
γ	$(\chi_g b_0^2/(\mu_m g r_0))$ dimensionless gamma parameter (–)
λ	thermal conductivity (W/(m K))
λ^{jelly}	thermal conductivity of jelly (W/(m K))
θ_0	reference temperature equal to 298 K (K)
θ_{cold}	cold wall temperature (K)
θ_{hot}	hot wall temperature (K)
μ	viscosity (Pa s)
μ_m	magnetic permeability in a vacuum (H/m)
ν	kinematic viscosity (m^2/s)
ρ	density (kg/m^3)
χ_g	mass magnetic susceptibility (m^3/kg)

Superscripts

fluid	the property related to the working fluid
jelly	the property related to the jelly

and the promotion of combustion [14] were found. The induction of magnetic convection in stably stratified air in a cube heated from above and cooled from below was presented by Kaneda et al. [7].

On the other hand, there are many works on the closed single-phase thermosyphon. Some of them are by Bayley and Lock [1], Japikse et al. [6], Mallinson et al. [11], Lock and Liu [9], Lock and Kirchner [8], Ishihara et al. [4,5]. They studied various geometrical configurations, fluid properties and thermal conditions of the system. A characteristic spoke pattern was observed in the middle cross-section (between the hot and cold parts of thermosyphon). It was described by Mallinson et al. [11] and Ishihara et al. [5]. They found that the number of spokes depended on the geometry, thermal properties of the system and the fluid properties. The number of spokes increased with increase in the Rayleigh number. Bayley and Lock [1] presented the heat transfer characteristics of the closed thermosyphon. They observed that increase in the Nusselt number is correlated with the increase in the Rayleigh number. The influence of geometry on the heat transfer was investigated by Lock and Liu [9]. They found that when the ratio of heated versus cooled length increased, the Nusselt number decreased (a similar observation was reported by Bayley and Lock [1]).

The stable configuration of the thermosyphon has not apparently been studied, due to its low heat transfer performance. Furthermore, the influence of magnetic field on the thermosyphon-like configuration has not been studied. Therefore, the effect of a magnetic field on the convection of paramagnetic fluid in the unstable (the lower wall heated and the upper wall cooled) and stable (the lower wall cooled and the upper wall heated) thermosyphon-like configurations is presented. Possible application includes the magnetic mixing of fluid even without a gravitational acceleration in a space.

2. Apparatus

The experimental enclosure in the stable configuration is presented in Fig. 1. In the unstable configuration, the cylinder was turned upside-down. The cylinder diameter

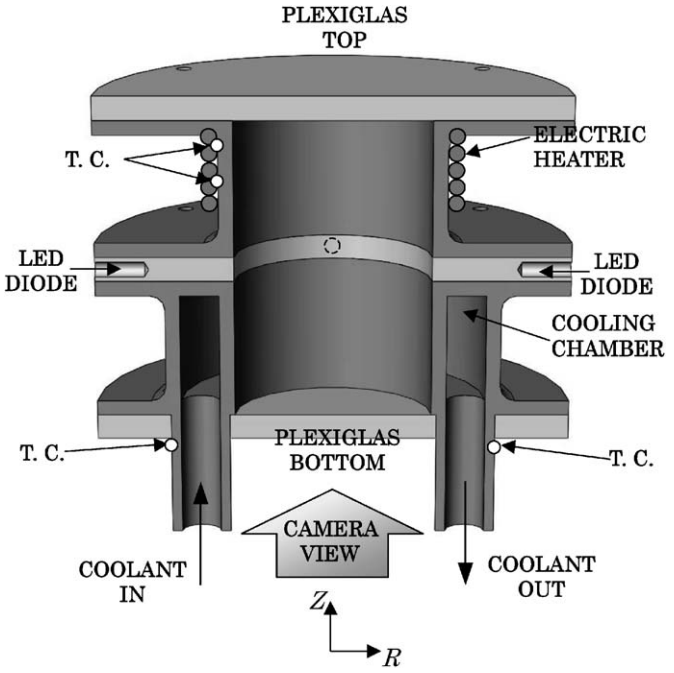

Fig. 1. Experimental enclosure in the stable configuration.

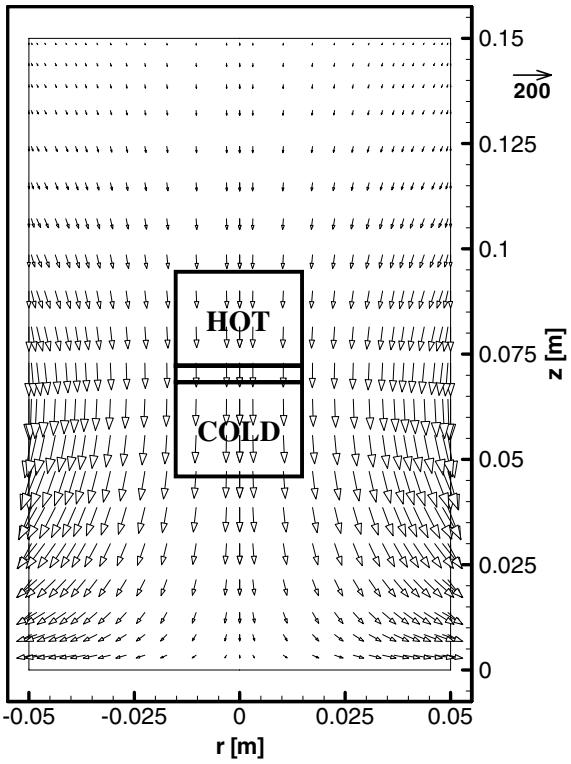

Fig. 2. Calculated vector profiles of $\vec{\nabla}b^2$ in the bore of superconducting magnet with the experimental enclosure shown schematically.

is 0.04 m and heated and cooled side walls are made of copper, are 0.028 m in height, and are separated by thin Plexiglas cylinder plate of 0.004 m in its thickness. Four holes were drilled from the side wall of this plate to place four high luminosity LED diodes (Nichia NSPW300BS) for visualization of the temperature field in the fluid.

The top and bottom end plates of cylinder were made of Plexiglas. In the top plate, a tiny hole was drilled through which the enclosure was filled with 50% volume aqueous solution of glycerol. Air bubbles remaining in the enclosure were removed by using a syringe with a very thin needle. The hole was also used to control the level of fluid in the enclosure, which changed due to the thermal expansion of the fluid.

The outside surface of the enclosure side wall was heated with a rubber-coated nichrome wire. The wire was connected to a DC power supply (Kikusui PAK 60-12A). The heating power (the current and voltage) was constantly recorded by two multimeters (Keithley 2000). The side wall of another cylinder was kept at a constant temperature with water pumped through a constant temperature bath. The temperature difference between the heated and cooled parts of the enclosure was measured with T-type Copper-Constantan thermocouples (marked in Fig. 1 as T.C.). Two thermocouples were located on the outer side of the heated wall, while another two were attached to the coolant outlet and inlet. The temperature data were recorded in a data logger (Keyence NR-1000). Both heated and cooled parts were thermally insulated with polystyrene foam.

The experimental cylinder, insulated with vinyl foil, was placed into the bore of helium-free 5 T superconducting magnet (HF5-100VHT). The middle height cross-section of the experimental cylinder was placed at 0.01 m from the opening level of the bore. This provides the minimum radial component of magnetic buoyancy force in the experimental fluid. The calculated vector profiles of $\vec{\nabla}b^2$ (proportional to the magnetic buoyancy force) are presented in Fig. 2, which demonstrates how the magnetic buoyancy force acts on the fluid in the experimental enclosure. Two configurations of the enclosure are presented in Fig. 3.

3. Working fluid

Isotherms in the middle-height cross-section were visualized by using a thermo-sensitive liquid crystal slurry dispersed in the glycerol solution. Glycerol itself is hard to handle; therefore an aqueous solution of glycerol was used. The concentration of glycerol affected the physical properties of the solution, especially the Prandtl number, defined as

$$Pr = \frac{\nu}{\alpha}. \tag{1}$$

The Prandtl number increases considerably when the concentration of glycerol is higher than 50%. Therefore the 50% volume concentration of glycerol in the solution was chosen as a working fluid.

Water and glycerol are diamagnetic fluids, as is the aqueous solution of glycerol. To increase the magnetic susceptibility of the working fluid and make it paramagnetic, gadolinium nitrate hexahydrate $Gd(NO_3)_3 \cdot 6H_2O$, was

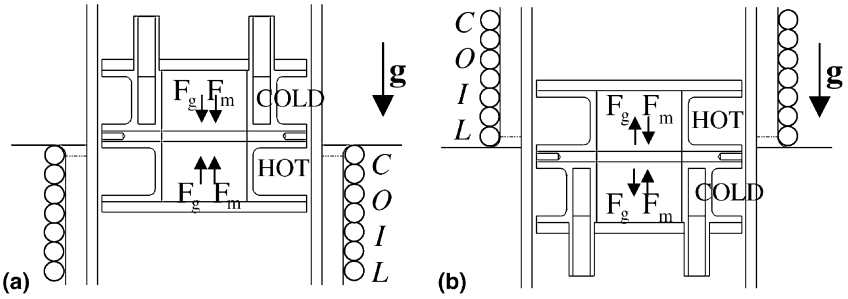

Fig. 3. Configurations of the system (F_g – the gravitational buoyancy force, F_m – the magnetic buoyancy force): (a) unstable and (b) stable.

Table 1
Properties of 50% volume aqueous solution of glycerol at $\theta_0 = 298$ K

Property	Value	Unit
α^*	1.1415×10^{-7}	m^2/s
β^*	0.445×10^{-3}	K^{-1}
λ^*	0.422	W/(m K)
μ	$6.145 \times 10^{-3} \pm 0.064 \times 10^{-3}$	Pa s
ν	$4.80 \times 10^{-6} \pm 0.05 \times 10^{-6}$	m^2/s
ρ	1281 ± 1	kg/m^3
χ_g	13.926×10^{-8}	m^3/kg

The properties marked by asterisk were estimated from [15].

dissolved in it at a molar concentration of 0.5 mol/(kg of solution). This corresponded to 225.7 g of gadolinium nitrate dissolved in 774.3 g of glycerol aqueous solution. The mass magnetic susceptibility of the working fluid was measured with a magnetic susceptibility balance (by the modified Gouy method known as the Evan's method) and was found to be $\chi_g = 13.926 \times 10^{-8}$ m^3/kg.

Density of the working fluid was measured by using a pycnometer and was found to be $\rho = 1281 \pm 1$ kg/m^3. An Ostwald's viscosimeter was used to measure the viscosity, which was $\mu = 6.145 \times 10^{-3} \pm 0.064 \times 10^{-3}$ Pa s. The properties of the working fluid at the temperature 298 K are summarized in Table 1 (properties marked with an asterisk were taken from [15]).

4. Experimental methods

In the experiment two main methods were utilized: visualization of the isotherms and the thermal measurements, as detailed below. Additional measurements related to the physical properties of working fluid (mentioned above) were also done.

4.1. Visualization

In order to investigate the influence of magnetic field on the flow mode and temperature field, the fluid temperature in the middle height cross-section was visualized with the liquid crystal slurries (KWN-2025, Japan Capsular Product Inc.). When illuminated by white light, the liquid crystals show different colors depending on the fluid temperature. Red indicates the lowest temperature, and blue the highest. In the present experiment, the red color corresponded to a temperature of about 291 K and the blue color to a temperature of about 294 K. A digital camera was used to record the images of isotherms in the chosen cross-section. The exposure time was 4 s.

Undesirable deposition of liquid crystal slurries on the walls was observed. It was necessary to withdraw the enclosure from the magnet bore and to shake it to recover the bright colors.

4.2. Thermal measurements

Thermal measurements were carried out to investigate the influence of magnetic field on the heat transfer rate. The Nusselt number is defined as follows:

$$Nu = \frac{Q_{\text{net\_conv}}}{Q_{\text{net\_cond}}}. \tag{2}$$

The net convection ($Q_{\text{net\_conv}}$) and net conduction ($Q_{\text{net\_ cond}}$) heat fluxes were estimated by the method invented by Ozoe and Churchill [12] and applied, e.g., in [10]. The net convection heat flux ($Q_{\text{net\_conv}}$) was estimated as the difference between the total heat supply during the convection experiment and the heat loss. The net conduction heat flux ($Q_{\text{net\_cond}}$) was estimated as the difference between the total heat supply during the conduction experiment and the heat loss. The heat loss was assumed to depend on the heater temperature itself and not on the mode of heat transfer inside the enclosure.

The empty thermosyphon-like enclosure was placed in the bore of the magnet and the heat loss to the environment was measured. The convection and conduction heat fluxes through air were neglected due to its low thermal conductivity.

Because of the complex geometry of the experimental system, the net conduction flux in the working fluid ($Q^{\text{fluid}}_{\text{net\_cond}}$) was measured as follows. Even in the stable configuration (see Figs. 1 and 3b), convection occurred near the side walls. Therefore, a jelly was used to obtain the conduction state in the enclosure. In the solidified jelly, heat transfer occurs only by conduction. The conduction heat flux through the working fluid for the same system was presumed to be approximated by the equation

$$Q^{\text{fluid}}_{\text{net\_cond}} = Q^{\text{jelly}}_{\text{net\_cond}} \frac{\lambda^{\text{fluid}}}{\lambda^{\text{jelly}}}. \tag{3}$$

The thermal conductivity of jelly λ^{jelly} was measured by using a cubical enclosure of internal size $a = 0.03$ m. The bottom wall was cooled, while the top wall was heated to establish conduction in the enclosure. The heating power and the temperature difference between the heated and cooled plates were recorded.

The heat loss from the heater attached to the cubical enclosure ($Q_{\text{loss\_cubic}}$) to the environment was also estimated with the empty cubical enclosure. The heat flux through the air in the enclosure was assumed to be negligible. The temperature difference between the hot and cold walls versus the total heat supply provides the heat loss line. Then the cubical enclosure was filled with a jelly, and after its coagulation the conduction experiment was performed. The thermal conductivity of the jelly could be estimated from the equation

$$\lambda^{\text{jelly}} a^2 \frac{(\theta_{\text{hot}} - \theta_{\text{cold}})}{a} = Q_{\text{heater}} - Q_{\text{loss\_cubic}}, \tag{4}$$

where $Q_{\text{heater}} = UI$, U is the voltage of heat supply, I the electric current of heat supply. $Q_{\text{loss\_cubic}}$ can be given from the heat loss line for the same temperature difference.

The Eq. (4) can be written in the form

$$\lambda^{\text{jelly}} = \frac{UI - Q_{\text{loss\_cubic}}}{a(\theta_{\text{hot}} - \theta_{\text{cold}})}. \tag{5}$$

Estimated value of the thermal conductivity of jelly was $\lambda^{\text{jelly}} = 0.575 \pm 0.040$ W/(m K).

The convection heat flux (Q_{conv}) was measured during the experiment for every case. The net conduction ($Q_{\text{net\_cond}}$) heat flux was estimated from Eq. (3), and net convection ($Q_{\text{net\_conv}}$) heat flux was estimated as the difference between the total power supply and heat loss. Then the Nusselt number was obtained from Eq. (2).

The utilization of the jelly in the conduction experiment can be applied to estimate the conduction heat flux for systems with complex geometry.

5. Experimental procedure

The experiment was carried out for the unstable and stable configurations of the enclosure (see Fig. 3). It was carried out also for various Rayleigh numbers defined as

$$Ra = \frac{g\beta(\theta_{\text{hot}} - \theta_{\text{cold}})r_0^3}{\alpha\nu} \tag{6}$$

and various strengths of the magnetic induction. The experimental procedure was the same for all cases in both configurations of the system.

The environmental temperature was kept at a constant level. First, the temperature of thermostating water and the power supply to the electric heater were set. The electric current and voltage of power supply for a heater were set at fixed values. The hot and cold wall temperatures were measured by thermocouples to provide the Rayleigh number. Temperature and visualized isotherms were first recorded after 90–120 min, when the system reached the steady state. Afterwards the magnetic field was applied to the system. The magnetic induction was changed from 1 T up to 5 T in steps of 1 T. Each step required around 40–60 min for the system to reach the steady state. Then the temperature, power supply and fluid flow structure were recorded. The recorded data were afterwards utilized for estimation of the Nusselt number, the Rayleigh number and the magnetic Rayleigh number defined as follows:

for unstable configuration

$$Ra_{\text{m}} = Ra\left[1 + \gamma\left(1 + \frac{1}{\beta\theta_0}\right)\left(B_z\frac{\partial B_z}{\partial Z}\right)\begin{matrix} r = 0 \\ z = 0 \end{matrix}\right], \tag{7}$$

for stable configuration

$$Ra_{\text{m}} = Ra\left[-1 + \gamma\left(1 + \frac{1}{\beta\theta_0}\right)\left(B_z\frac{\partial B_z}{\partial Z}\right)\begin{matrix} r = 0 \\ z = 0 \end{matrix}\right]. \tag{8}$$

6. Experimental results

In the unstable configuration (see Fig. 3a), convective flow was obtained without a magnetic field. It resulted in the appearance of a spoke pattern in the adiabatic zone between the heated and cooled parts. Fig. 4 shows the visualized isotherms for selected Rayleigh numbers and selected strengths of magnetic induction. The first column in Fig. 4a–c at 0 T (without a magnetic field) presents the effect of Rayleigh number on the convective flow in the system. The spoke pattern is apparent. The blue (dark) color corresponds to the highest temperature, and the red (light color) area corresponds to lower temperature. These pictures indicate the hot rising flow in the blue area and the cold descending flow in the red area. This flow mode is typical of the unstable thermosyphon configuration. Depending on the Rayleigh number, various numbers of spokes appeared: in Fig. 4a at $Ra_0 = 1.69 \times 10^5$, five spokes; in Fig. 4b at $Ra_0 = 2.38 \times 10^5$, six spokes; and in Fig. 4c at $Ra_0 = 3.36 \times 10^5$, seven spokes. The number of spokes increased with increase in the Rayleigh number.

The series of pictures in Fig. 4 clearly indicate the enhancing effect of the magnetic field on convection, even for the weak magnetic field of 1 T. Both magnetic and gravitational buoyancy forces act in the same direction, as shown schematically in Fig. 3a. The cold fluid in the upper cold region was attracted to the strong magnetic field. Simultaneously, it sank due to its higher density. The hot fluid was repelled upwards from the high magnetic field and also driven upwards by the gravitational buoyancy force. This joint effect induced a strong convective flow and resulted in multiplication of the angular spokes with the increase in applied magnetic field. The number

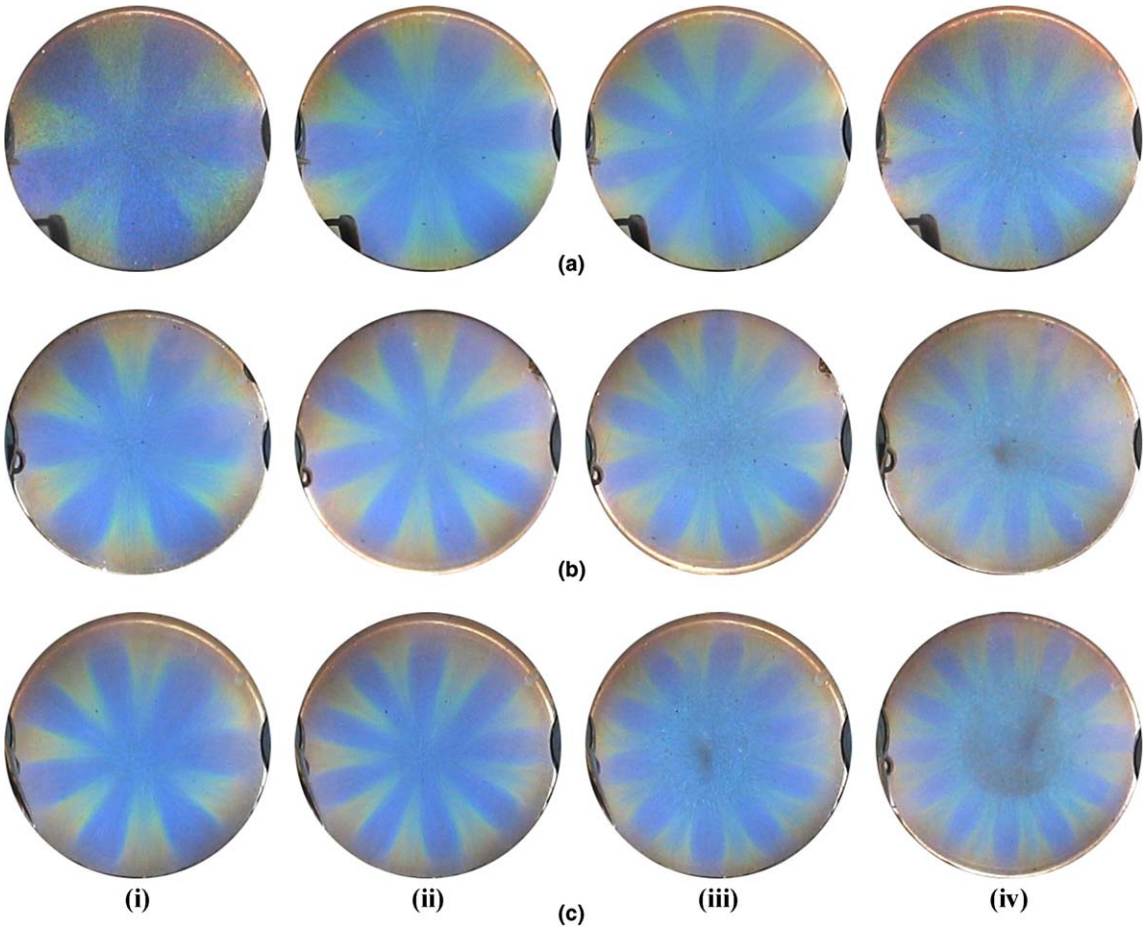

Fig. 4. Isotherms for various strengths of the magnetic field in the unstable configuration: (a) Case u3, $Ra_0 = 1.69 \times 10^5$, (b) Case u4, $Ra_0 = 2.38 \times 10^5$, (c) Case u5, $Ra_0 = 3.36 \times 10^5$. (i) 0 T, (ii) 1 T, (iii) 2 T, (iv) 3 T.

of spokes increased for Case u3 at $Ra_0 = 1.69 \times 10^5$ from 5 to 7, for Case u4 at $Ra_0 = 2.38 \times 10^5$ from 6 to 12 and for Case u5 at $Ra_0 = 3.36 \times 10^5$ from 7 to 12 when the magnetic induction was increased from 0 T to 3 T. Six spokes were obtained for Case u3 at $Ra_0 = 1.69 \times 10^5$ and 1 T and for Case u4 at $Ra_0 = 2.38 \times 10^5$ without magnetic field. This suggests that the convective flow for Case u3 under the magnetic field is similar to that for Case u4 without magnetic field. At the magnetic induction of 2 T, the number of spokes (for Case u3 at $Ra_0 = 1.69 \times 10^5$) becomes 9, which is larger than 7 spokes for Case u5 at $Ra_0 = 3.36 \times 10^5$ and 0 T. This means that the increase in the magnetic field strength is more effective than the gravitational buoyancy force in enhancing the convection even with half of the temperature difference between the heated and cooled walls. The numbers of spokes versus the maximum magnetic induction for the cases in the unstable configuration (listed in Table 2) are presented in Fig. 5. The increase in the number of spokes due to the magnetic field is apparent.

The system configuration (shown in Figs. 1 and 3b) is thermally stable unless the magnetic field is applied. The gravitational buoyancy force causes the temperature stratification with slight convective flow near the vertical side

Table 2
Experimental results for the system in the unstable configuration

Configuration	Case	Initial Rayleigh number, $Ra_0 \times 10^{-5}$	Maximum magnetic induction, number of spokes					
			0 T	1 T	2 T	3 T	4 T	5 T
Unstable	Case u1	0.23	3	4	5	6	8	8
	Case u2	0.43	4	5	6	7	8	10
	Case u3	1.69	5	6	9	11	13	14
	Case u4	2.38	6	8	9	12	14	15
	Case u5	3.36	7	9	10	12	14	17

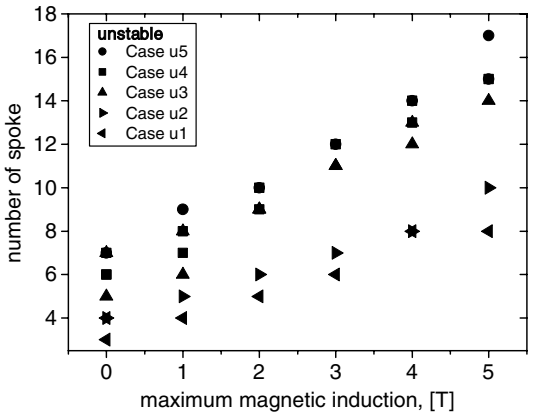

Fig. 5. Observed number of spokes in the unstable configuration of the system for various strengths of the maximum magnetic induction (Case u1 at $Ra_0 = 0.23 \times 10^5$, Case u2 at $Ra_0 = 0.43 \times 10^5$, Case u3 at $Ra_0 = 1.69 \times 10^5$, Case u4 at $Ra_0 = 2.38 \times 10^5$ and Case u5 at $Ra_0 = 3.36 \times 10^5$).

wall. The hot fluid stayed in the heated, upper part of enclosure, while the cold fluid remained in the cooled, lower part due to its higher density. It resulted in a stagnant, almost conduction state. Fig. 6 shows the visualized isotherms for selected Rayleigh numbers and selected strengths of magnetic induction for the system in the stable configuration. The pictures in Fig. 6a–c at 0 T were taken for various Rayleigh numbers without magnetic field. The uniform color of the pictures indicates the presence of an isothermal layer of fluid in the mid-height region. The color indicates the mean fluid temperature. The spoke pattern was not observed.

With the increase in the magnetic strength, the magnetic buoyancy force gradually outweighed the gravitational buoyancy force. When the level of 2 T was achieved, the spokes appeared suddenly in the visualized cross-section. For Case s4 at $Ra_0 = 2.79 \times 10^5$ and 2 T, 7 spokes suddenly appeared. This suggests that the magnetic field drove the convection in the same way as the gravitational field for Case u5 at $Ra_0 = 3.36 \times 10^5$ (the unstable configuration at 0 T, see Fig. 4c). The number of spokes increased for Case s4 at $Ra_0 = 2.79 \times 10^5$ from 0 to 10, for Case s5 at $Ra_0 = 3.80 \times 10^5$ from 0 to 11 and for Case s6 at $Ra_0 = 5.22 \times 10^5$ from 0 to 11 with increase in the magnetic induction from 0 T to 3 T. The number of spokes versus the maximum magnetic induction for the cases in stable configuration listed in Table 3 is presented in Fig. 7.

Fig. 8 shows a series of instantaneous isotherms in the stable thermosyphon configuration at $Ra_0 = 5.22 \times 10^5$

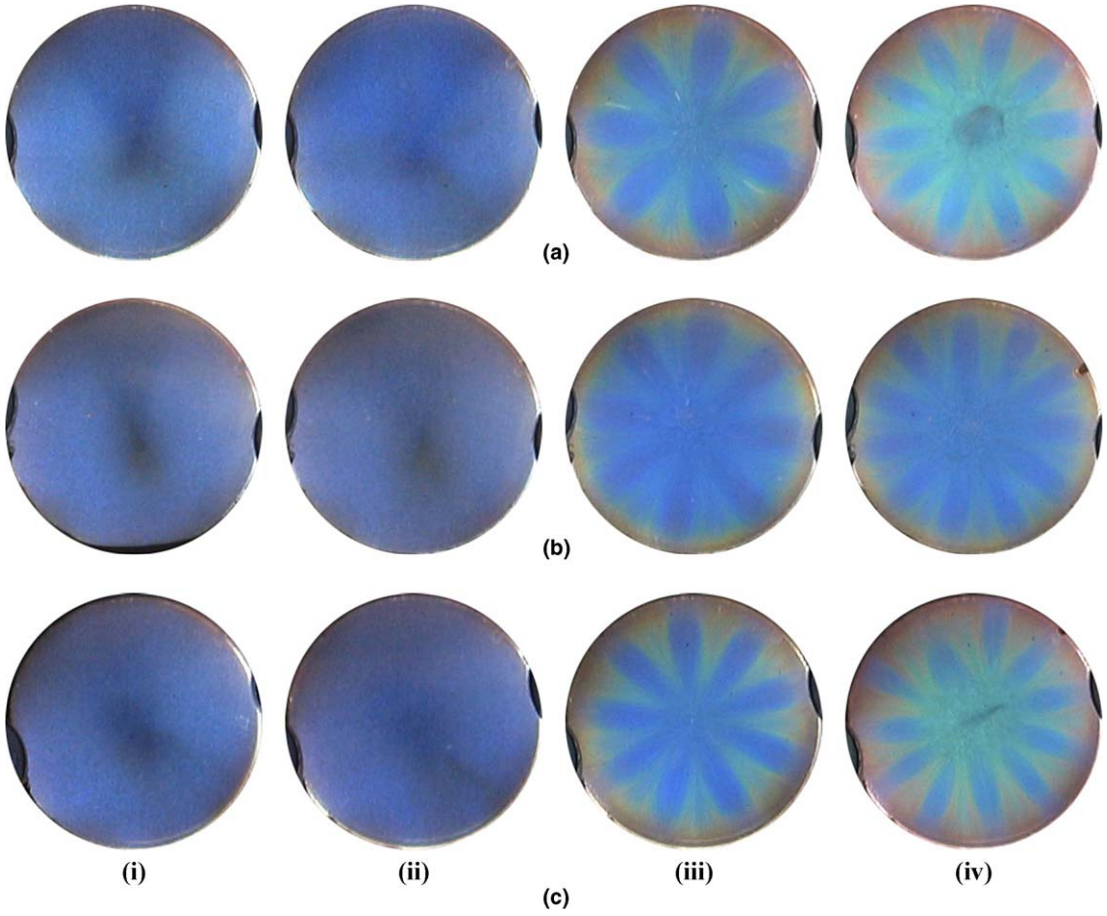

Fig. 6. Isotherms for various strengths of the magnetic field in the stable configuration. (a) Case s4, $Ra_0 = 2.79 \times 10^5$, (b) Case s5, $Ra_0 = 3.8 \times 10^5$, (c) Case s6, $Ra_0 = 5.22 \times 10^5$. (i) 0 T, (ii) 1 T, (iii) 2 T, (iv) 3 T.

Table 3
Experimental results for the system in the stable configuration

Configuration	Case	Initial Rayleigh number, $Ra_0 \times 10^{-5}$	Maximum magnetic induction, number of spokes					
			0 T	1 T	2 T	3 T	4 T	5 T
Stable	Case s1	0.14	0	0	4	5	6	8
	Case s2	0.36	0	0	3	5	7	8
	Case s3	2.57	0	0	7	10	12	14
	Case s4	2.79	0	0	7	10	13	14
	Case s5	3.80	0	0	8	11	13	15
	Case s6	5.22	0	0	9	11	13	17

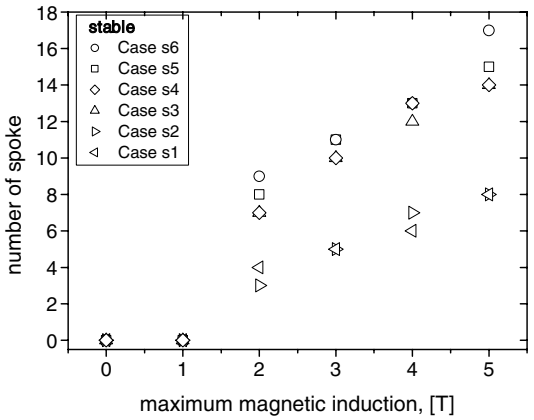

Fig. 7. Observed number of spokes in the stable configuration of the system for various strengths of the maximum magnetic induction (Case s1 at $Ra_0 = 0.14 \times 10^5$, Case s2 at $Ra_0 = 0.36 \times 10^5$, Case s3 at $Ra_0 = 2.57 \times 10^5$, Case s4 at $Ra_0 = 2.79 \times 10^5$, Case s5 at $Ra_0 = 3.80 \times 10^5$ and Case s6 at $Ra_0 = 5.22 \times 10^5$).

after a step change in the magnetic induction from 1 T to 2 T. It should be emphasized that the magnetic field increased gradually and reached the level of 2 T after 90 s. The first picture marked $t = 0$ s was taken just before changing the magnetic field and is therefore a reference image for the transient fluid flow.

In Fig. 8 at $t = 72$ s (before the level of 2 T was reached), the heated fluid (represented by the circular blue color) was repelled from the coil and flowed downward in the centre of enclosure. Simultaneously, the cooled fluid (represented by the brown color) was attracted to the coil and flowed upward. It looked as if a "hot plume" of fluid moved downward and then the system started to reach some kind of balance and the spoke pattern appeared. The streams of heated and cooled fluid were advected against each other, and finally the alternate seven spoke pattern was resulted (at $t = 784$ s). These transient pictures demonstrate how fast the magnetic field induces convection. At magnetic induction of 1 T, the gravitational buoyancy force appeared to be of the same order as the magnetic buoyancy force. At the magnetic induction of 2 T, the magnetic buoyancy force becomes dominant.

Figs. 9 and 10 compare the unstable and stable configurations of the thermosyphon. The number of spokes versus the magnetic Rayleigh number is shown in Fig. 9. The values of magnetic Rayleigh numbers for the maximum magnetic induction $b = 0$, 1, 2, 3, 4 and 5 T for the unstable and stable configurations of the system are listed in Tables 4 and 5, respectively. In both configurations, increase in the magnetic Rayleigh number causes increase in the number of spokes. For the strongest magnetic field (5 T), the number of spokes almost agrees in both configurations. The numbers of spokes for both configurations takes rather wide range but it tends to converge to each other for the larger magnetic Rayleigh number, which suggest that the magnetic buoyancy force dominates the system.

Fig. 10 compares the Nusselt number for the unstable and stable configurations of the thermosyphon versus the magnetic Rayleigh number. Increase in the magnetic Rayleigh number resulted in increase in the Nusselt number. For the stable configuration, Nusselt numbers near two can be observed for negative values of the magnetic Rayleigh number. This value of the Nusselt number suggested that it was not possible to obtain the conduction state even for the stable configuration of the system, but a near-conduction state was achieved. For the unstable configuration of the thermosyphon, the near-conduction state was not observed.

The magnetic Rayleigh number was originally introduced by Braithwaite et al. [2] for a Rayleigh–Benard convection of a horizontal fluid layer heated from below and cooled from above and it may be an extension to use it for the present thermosyphon configuration. But the general trend of the number of spokes and the average Nusselt number are roughly correlated with the magnetic Rayleigh number as shown herein both for the unstable and stable systems. The magnetic Rayleigh number appears to be useful as one of the measure for the thermosyphon-like configuration as studied herein.

7. Conclusions

Experimental flow visualizations and the heat transfer rates are presented for a single-phase thermosyphon in unstable and stable configurations under various thermal and magnetic conditions. For the unstable configuration, convective flow was observed without a magnetic field, and a spoke pattern appeared in the middle-height cross-section. Increase in the Rayleigh number resulted in larger numbers of spokes, which means convective flow was enhanced. Increasing magnetic strength in the unstable

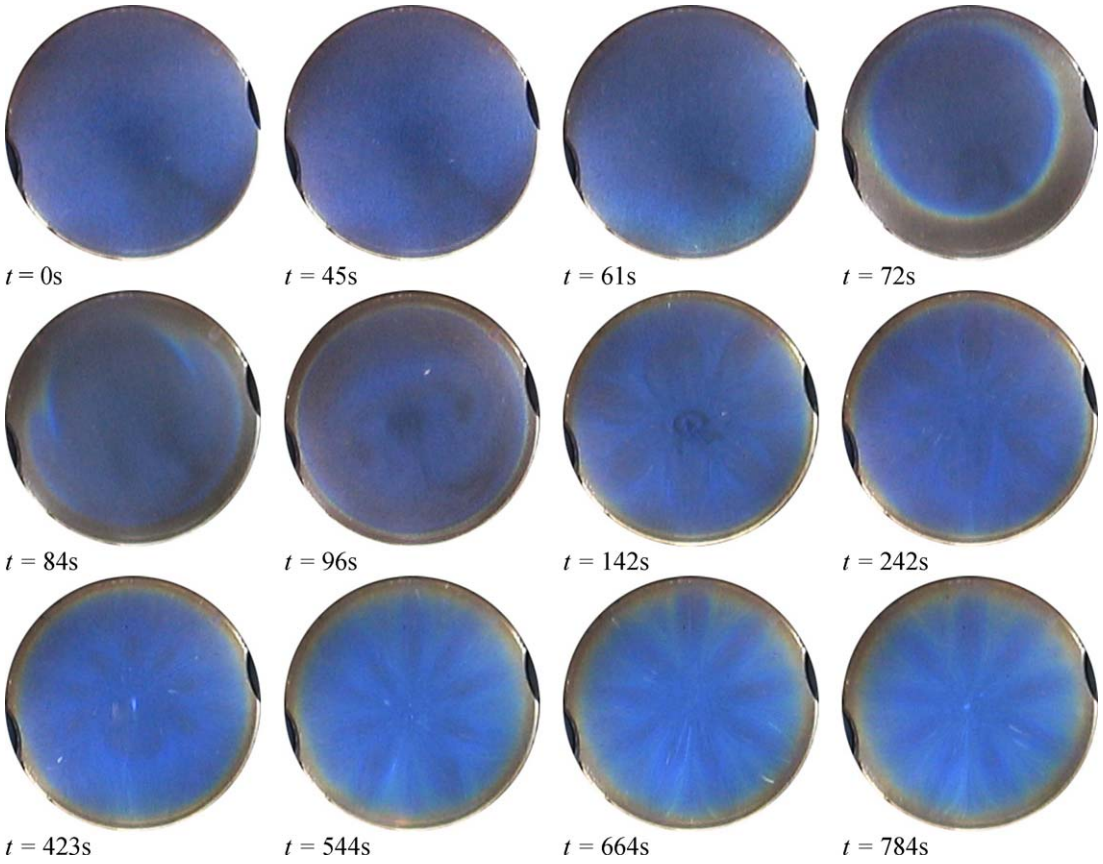

Fig. 8. A series of instantaneous isotherms for Case s6 at $Ra_0 = 5.22 \times 10^5$, after a step change from 1 T to 2 T.

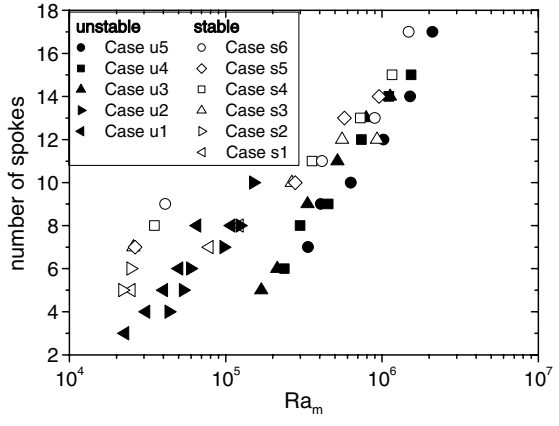

Fig. 9. Observed number of spokes versus the magnetic Rayleigh number for the unstable (Case u1 at $Ra_0 = 0.23 \times 10^5$, Case u2 at $Ra_0 = 0.43 \times 10^5$, Case u3 at $Ra_0 = 1.69 \times 10^5$, Case u4 at $Ra_0 = 2.38 \times 10^5$ and Case u5 at $Ra_0 = 3.36 \times 10^5$) and stable (Case s1 at $Ra_0 = 0.14 \times 10^5$, Case s2 at $Ra_0 = 0.36 \times 10^5$, Case s3 at $Ra_0 = 2.57 \times 10^5$, Case s4 at $Ra_0 = 2.79 \times 10^5$, Case s5 at $Ra_0 = 3.80 \times 10^5$ and Case s6 at $Ra_0 = 5.22 \times 10^5$) configurations of the system.

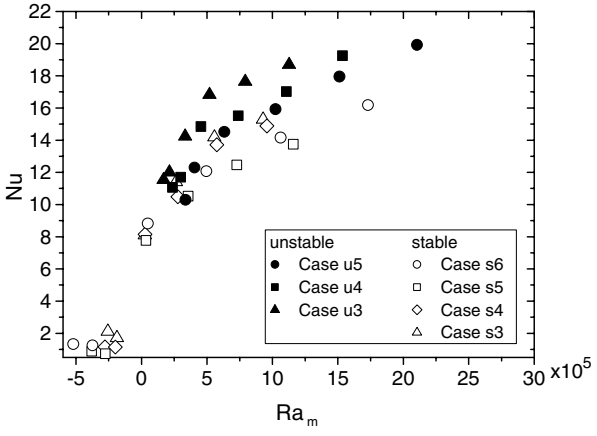

Fig. 10. Comparison of the Nusselt number versus the magnetic Rayleigh number for the unstable (Case u3 at $Ra_0 = 1.69 \times 10^5$, Case u4 at $Ra_0 = 2.38 \times 10^5$ and Case u5 at $Ra_0 = 3.36 \times 10^5$) and stable (Case s3 at $Ra_0 = 2.57 \times 10^5$, Case s4 at $Ra_0 = 2.79 \times 10^5$, Case s5 at $Ra_0 = 3.80 \times 10^5$ and Case s6 at $Ra_0 = 5.22 \times 10^5$) configurations of the system.

configuration also resulted in larger numbers of spokes. In accordance with the similar effect of increasing Rayleigh number, it can be said that the increasing magnetic field enhanced the convective flow. For the stable system configuration, convective flow was not observed in the absence of a magnetic field, and the Rayleigh number had no discernible influence on the flow structure. After applying the magnetic field, convective flow was obtained. It was found that the magnetic buoyancy force of about 1 T appears to be equal to the gravitational buoyancy force. A magnetic

Table 4
Magnetic Rayleigh number for the system in the unstable configuration

Configuration	Case	Initial Rayleigh number, $Ra_0 \times 10^{-5}$	Maximum magnetic induction, magnetic Rayleigh number $Ra_m \times 10^{-5}$					
			0 T	1 T	2 T	3 T	4 T	5 T
Unstable	Case u3	1.69	1.69	2.14	3.34	5.19	7.92	11.28
	Case u4	2.38	2.38	2.99	4.53	7.39	11.07	15.36
	Case u5	3.36	3.36	4.06	6.33	10.24	15.13	21.04

Table 5
Magnetic Rayleigh number for the system in the stable configuration

Configuration	Case	Initial Rayleigh number, $Ra_0 \times 10^{-5}$	Maximum magnetic induction, magnetic Rayleigh number $Ra_m \times 10^{-5}$					
			0 T	1 T	2 T	3 T	4 T	5 T
Stable	Case s3	2.57	−2.57	−1.87	0.25	2.65	5.56	9.28
	Case s4	2.79	−2.79	−2.00	0.26	2.78	5.75	9.58
	Case s5	3.80	−3.80	−2.76	0.35	3.57	7.28	11.60
	Case s6	5.22	−5.22	−3.74	0.48	4.96	10.63	17.30

field greater than 1 T induced the convective flow. In the present experiment, the induction of convective flow resulted in the appearance of a spoke pattern in the mid-height adiabatic zone and also in increase of the Nusselt number. The Nusselt number obtained for the unstable configuration of the thermosyphon was slightly higher than that for the stable configuration. Convection inside the closed thermosyphon system may be controllable by use of a magnetic field. A strong magnetic field was able to enhance (in the unstable configuration) and to induce (in the stable configuration) convective flow in the system.

Acknowledgements

A part of this work was supported by European Commission (Project Dev-CPPS, FP6 – No. 002968).

References

[1] F.J. Bayley, G.S.H. Lock, Heat transfer characteristics of the closed thermosyphon, J. Heat Transfer 87 (1965) 30–40.
[2] D. Braithwaite, E. Beaugnon, R. Tournier, Magnetically controlled convection in a paramagnetic fluid, Nature 354 (1991) 134–136.
[3] Y. Ikezoe, N. Hirota, J. Nakagawa, K. Kitazawa, Making water levitate, Nature 393 (1998) 749–750.
[4] I. Ishihara, T. Fukui, R. Matsumoto, Natural convection in a vertical rectangular enclosure with symmetrically localized heating and cooling zones, Int. J. Heat Fluid Flow 23 (2002) 366–372.
[5] I. Ishihara, R. Imanishi, M. Fujiwara, R. Matsumoto, Natural convection in a single-phase closed thermosyphon, in: Proceeding of the 10th International Symposium on Flow Visualization, Kyoto, 2002.
[6] D. Japikse, P.A. Jallouk, E.R.F. Winter, Single-phase transport processes in the closed thermosyphon, Int. J. Heat Mass Transfer 14 (1971) 869–887.
[7] M. Kaneda, T. Tagawa, H. Ozoe, Convection induced by a cusp-shaped magnetic field for air in a cube heated from above and cooled from below, J. Heat Transfer 124 (2002) 17–25.
[8] G.S.H. Lock, J.D. Kirchner, Some characteristics of the inclined, closed tube thermosyphon under low Rayleigh number conditions, Int. J. Heat Mass Transfer 35 (1) (1992) 165–173.
[9] G.S.H. Lock, Y. Liu, The effect of geometry on the performance of the closed tube thermosyphon at low Rayleigh numbers, Int. J. Heat Mass Transfer 32 (6) (1989) 1175–1182.
[10] S. Maki, T. Tagawa, H. Ozoe, Enhanced convection or quasi-conduction states measured in a super conducting magnet for air in a vertical cylindrical enclosure heated from below and cooled from above in a gravity field, J. Heat Transfer 124 (4) (2002) 667–673.
[11] G.D. Mallinson, A.D. Graham, G. de Vahl Davis, Three-dimensional flow in a closed thermosyphon, J. Fluid Mech. 109 (1981) 259–275.
[12] H. Ozoe, S.W. Churchill, Hydrodynamic stability and natural convection in newtonian and non-newtonian fluids heated from below, AIChE Symp. Ser. Heat Transfer 69 (1973) 126–133.
[13] M. Wakayama, N.I. Wakayama, Magnetic acceleration of inhaled and exhaled flows in breathing, Jpn. J. Appl. Phys. 39 (2000) 262–264.
[14] N.I. Wakayama, Magnetic promotion of combustion in diffusion flames, Combust. Flame 93 (1993) 207–214.
[15] VDI-Wärmeatlas, VDI-Verlag, 1997.